Machine learning implementation for in-orbit RSO orbit estimation using star tracker cameras

Siddharth Dave
York University

Ryan Clark, Gabriel Chianelli, Regina Lee
York University

ABSTRACT

The growing number of resident space objects (RSOs) in low Earth orbit (LEO) presents a concern for the future of our planet's space industry. The US space surveillance network (SSN) currently detects, tracks and catalogues upwards of 20,000 RSOs using a suite of dedicated ground and space-based sensors. A potential optical source of dispersed in-orbit space data for space situational awareness (SSA) are star trackers, a commonly found attitude determination instrument on satellites. This paper discusses the results of a novel recurrent convolutional neural network (R-CNN) based algorithm designed to make position and velocity estimates of in-orbit RSOs captured by a commercial-grade star tracker. Due to the low-resolution quality of star tracker images, the designed algorithm takes advantage of the high frame rate and short exposure time to estimate RSO position and velocity in orbit. Furthermore, by characterizing the streak patterns obtained from image sequences, followed by a deconvolution of star tracker attitude changes and orbital motion, relative position and velocity estimates can be achieved. The R-CNN design initially trains on synthetically generated noiseless images and is validated by images generated using an analytical image simulator. The objective of this research is to discuss how the designed algorithm can facilitate RSO orbit estimation for SSA using low-resolution star tracker. Preliminary results indicate that sub-pixel estimation and exposure-time streaks of RSOs from star tracker images are viable candidates for position and velocity estimation.

1. INTRODUCTION

Observation-based space situational awareness (SSA) is of key interest to the space industry. The increasing number of artificial objects in Earth orbit necessitates the continuous monitoring of the position and velocities of all these objects to minimize potential threats to space assets and human lives. The Space Surveillance Network (SSN) has detected over 20 000 objects in near Earth orbit and tracks and catalogs them using a suite of dedicated ground and space-based sensors. As identified by April [1], the lack of geographical distribution of SSN sensors is an important limiting factor in the current system. In this paper, we propose the novel approach of using low-resolution cameras, such as a space-borne star tracker, to augment the SSN for object detection and tracking.

1.1. FEASIBILITY OF RSO DETECTION USING STAR TRACKERS

A star tracker is an optical instrument commonly used on satellites for attitude determination. As a satellite orbits Earth, the star tracker takes periodic images of stars, called "star field images" in this paper. Using a catalogue of stars stored in memory, an automated algorithm estimates the boresight unit vector of the star tracker camera in the International Celestial Reference Frame to obtain the absolute attitude of the satellite. Various articles describe the design and operation of star trackers in attitude determination algorithms [2–4]. Star trackers occasionally image resident space object (RSO) streaks within the star field images. A recently conducted feasibility study using an analytical image simulator concluded that in LEO star tracker cameras are a feasible source for between 1 and 100 RSO detections per day, depending on the orientation and optical properties of the star trackers [5]. In this paper, we propose an algorithm based on machine learning to detect and then estimate RSO position from low-resolution images such as star tracker data. The focus of the current study is to determine the accuracy of RSO position estimation using star field images with RSO detections.

In order to validate the proposed algorithm, we used a series of simulated star field images. The image simulator used in this study is a custom Space-Based Optical Image Simulator (SBOIS) [6] calibrated using the Fast Auroral Imager (FAI), an optical instrument on the CASSIOPE satellite as part of the ePOP (Enhanced Polar Outflow Probe) science mission. SBOIS has been proven to replicate FAI images and RSO detections from previously published work by Clemens et al. [5] and has been improved since their initial work to allow for RSO shape, attitude, and host

satellite ephemeris data to improve the accuracy of the generated images. Integrating a parallel SGP4 computation structure as outlined in [6] allows for the generation of star field images considering the entire LEO catalog in a matter of seconds on a commercial computer.

1.2. MACHINE LEARNING IMPLEMENTATION

As with many image-based algorithms, the image frames must be converted into an accurate vector space representation to interpret the motion of both the observer and the observed. Within the scope of machine learning, image processing algorithms identify, classify, and characterize motion associated with objects like how the human brain functions. However, the small angular size of RSOs, which ranges between 2 and 10 seconds of arc, inhibit motion interpretation.

Our approach is to determine each RSO's spatiotemporal vector space projection onto the image plane. The image plane, as shown in Fig. 1(b), is defined as a 2D circular disk onto which RSO and star detections are visible, representative of the CCD (charge-coupled device). With temporal data of the host satellite's position in orbit, attitude, and camera mount offset, it is possible to estimate the RSO's relative and absolute position and velocity in an Earth-centered inertial frame of reference (ECI), hereafter referred to as "position state vector." To convert from image sequences, as shown in Fig. 1(a), to sub-pixel positions of detected objects with labels, we studied existing algorithm designs.

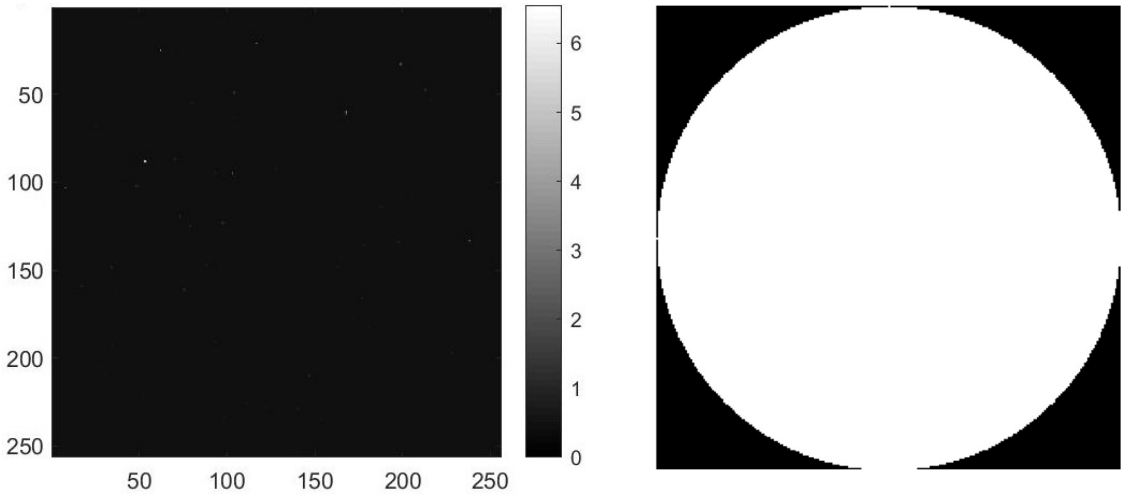

(a) (b)

Fig. 1 (a) A star-field image generated by the image simulator; (b) the camera's circular image plane

There have been several studies on space object classification and characterization using machine learning algorithms. Jia [7] classified light curves (brightness of an object over a period) but demonstrated only with the star images (not RSO data). Linares [8] approached the problem with Convolutional Neural Networks (CNN), and Muratov [9] used a deep neural network for satellite model determination. Zimmer [10] demonstrated the potential for smaller imaging platforms to contribute RSO measurements toward LEO debris and nanosatellite detections. Other optical ground and space-based observations indicate that a wide field-of-view optical instrument can track RSOs using streak detection. Cruces [11] presented a CNN design for RSO streak detection in wide field-of-view images. This method is part of a larger tracking strategy based on the sidereal motion from ground observations. Specific to space-based space surveillance, Scott [12] presents the key findings of the Near-Earth Object Surveillance Satellite (NEOSSat), a dedicated Canadian contribution to detecting and tracking asteroids and satellites using a 15 cm telescope. Scott identifies that NEOSSat is well suited for geostationary space surveillance; however, for LEO surveillance a more responsive system is required that can adapt to changing situations in real time with a faster image frame rate and shorter exposure times. (NEOSSat has a 100 s exposure time.) While these

studies suggest promising outcomes, the training of their algorithms and validation are based on relatively high-resolution ground and space-based observations. We propose a novel, recurrent convolutional neural network (R-CNN) design for low-resolution images, which is described in section 2.

1.3. IMAGE SPACE TO STATE VECTORS

Using the SBOIS, we generated sequential frames of 256 × 256 pixels at 1 and 0.5 Hz, which is a common star tracker frame rate. Although the angular size of the stars and RSOs is in arcseconds, the point spread function of the optical sensor causes the objects to appear like a 2D Gaussian of up to 20 arcminutes in size or localized to a 3 × 3-pixel square. For orbital estimation to work, our machine learning implementation must find the object's sub-pixel position.

The sub-pixel position and its estimation error define the parameters of a cone extending from the body frame of the host satellite toward the RSO, as shown in Fig. 2. The height of the cone (length of the red arrow) represents the distance to the RSO, and θ represents the estimated accuracy of the sub-pixel position. Using SBOIS, we generate a vector from the host satellite to the RSO to determine our algorithm's accuracy. For estimating a star's sub-pixel position, we validate the unit vector with a bright star catalog [13].

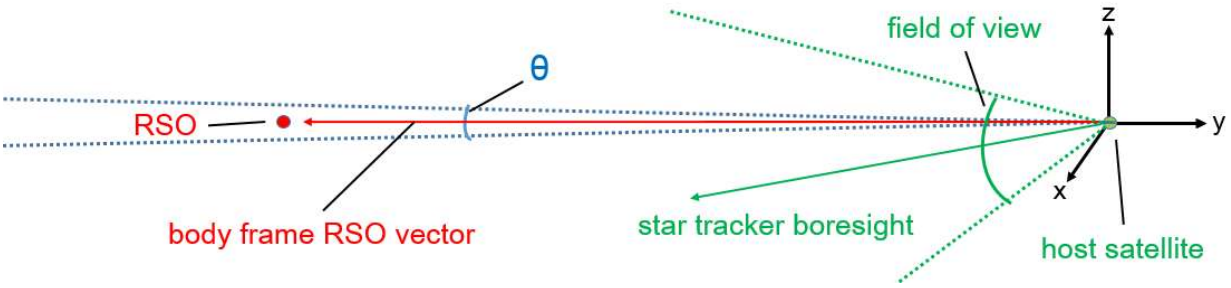

Fig. 2 The RSO sub-pixel estimation error is represented as θ, defined along the body frame RSO vector.

Every new image frame generated is a representation of a dynamic cone—the cone changes in height, angle θ, point of origin, and body frame RSO vector from one frame to the next (Fig. 3). As a dedicated and active RSO tracking sensor, NEOSSat can actively change its attitude to match the body frame vector to the RSO [12]. In our implementation, the star tracker is not a dedicated sensor, and the body frame RSO vector is offset by the host satellite attitude. Therefore, we first perform attitude estimation.

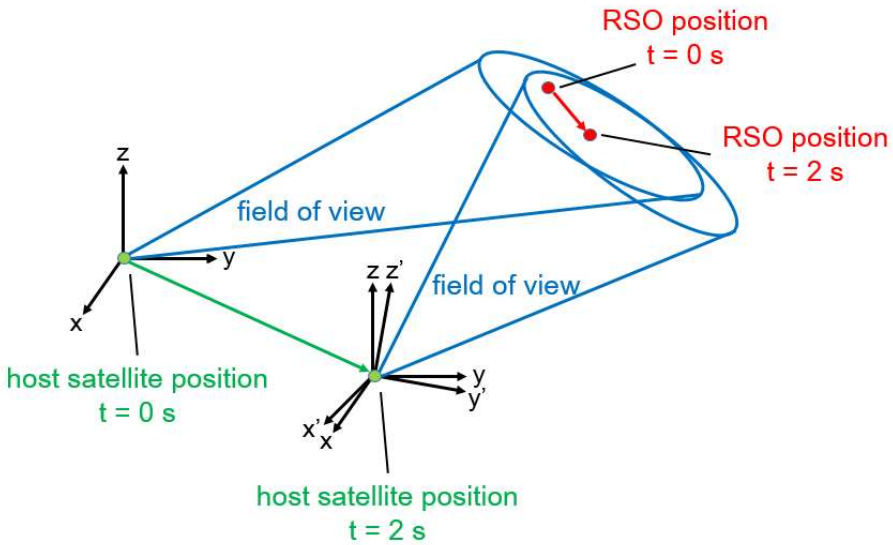

Fig. 3 Representation of an RSO's position displacement on the image plane of the host satellite with changing attitude and position

Attitude determination is the estimation of a spacecraft's orientation, typically the yaw, pitch, and roll values, relative to a known frame of reference. This requires line-of-sight measurements from the host satellite body frame of reference and the corresponding line-of-sight measurements within an inertial reference frame. Methods described in [14][15] are then used to calculate the rotation between these measurement vectors, which is equivalent to the coordinate transformation from the inertial frame to the body frame of reference. In this paper, the Quaternion Estimator (QUEST) algorithm is used for the attitude determination due to its computational speed [14]. For a star tracker, the body measurement vectors are found by first determining the sub-pixel locations of multiple stars in the image through our machine learning algorithm described in section 2. These pixel values are then converted to 3D Cartesian vectors using a predefined projection method described in [15][16]. Next, using methods defined in [17], a catalog-matching algorithm correlates the selected stars within the image to their star catalog IDs with known vectors in the inertial coordinate system. Finally, an attitude determination algorithm can be applied to these sets of vectors to estimate the attitude of the spacecraft relative to the inertial coordinate system [14].

As an RSO crosses the host satellite's image plane, the angular velocity is a projection of the changing body frame RSO vector. The change in the body frame RSO vector is dependent on the host satellite attitude and the position state vector of the host satellite and RSO in the Earth-centered inertial frame of reference. Our objective is to estimate the RSO position state vector in the inertial frame using the host satellite position state vector and body frame RSO vector.

Assuming the host satellite position state vector is known, the RSO position state vector is the addition of the body frame RSO vector and the host satellite position state vector (Fig. 4) [18]. Using the SBOIS, we validate our estimation of the RSO position state vector by comparing it to the RSO state vector generated by the simulator's orbital propagator.

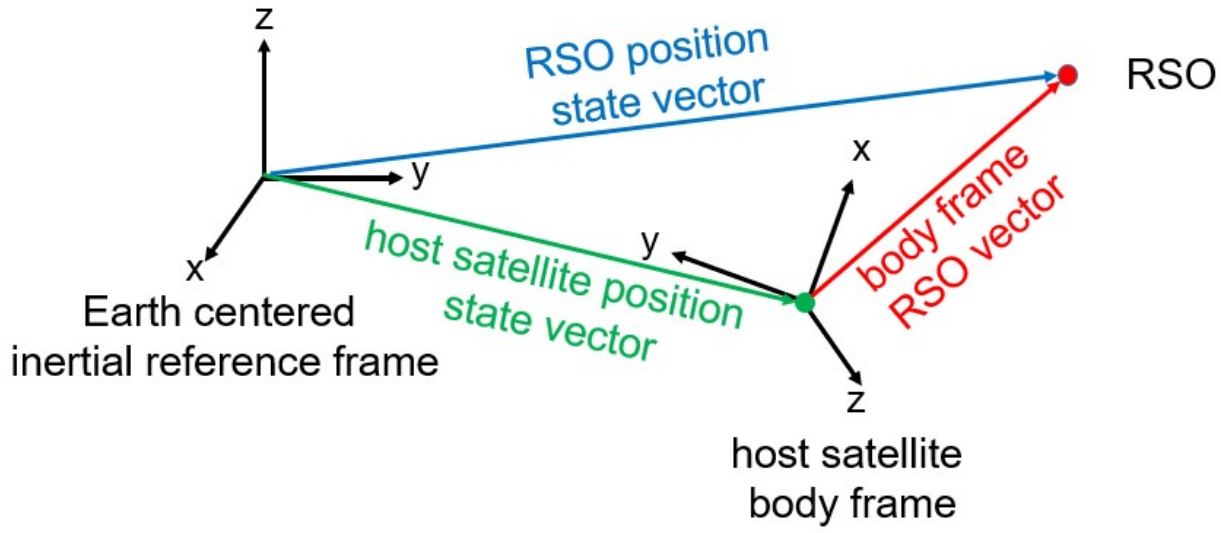

Fig. 4 Estimating the RSO state vector using the host satellite state vector and the body frame RSO vector

In using CASSIOPE as our host satellite model, the SBOIS incorporates the FAI imager's parameters and its body frame orientation. Using the nadir *x*-axis of CASSIOPE's body frame for reference, the FAI imager's boresight is offset by –60° in the *x*-axis and –90° in the *y*-axis. Knowledge of this offset allows us to convert the body frame RSO vector to an inertial frame [19]. The camera boresight, a body frame vector, is the line of sight of the camera extending forward from the center of the image plane. The boresight, alongside the planar *x* and *y* pixel coordinates, can be used as the orthogonal coordinates when converting from 2D pixel measurement values to 3D measurement vectors and vice versa. To estimate the body frame RSO vector using sub-pixel positions, we first identify the major

components that affect the sub-pixel position from one frame to the next. The change in position of an RSO on the image sequence is attributed to three factors: host satellite attitude change, RSO parallax (a component of host satellite orbital displacement and distance to RSO), and RSO orbital displacement. Our approach is to perform attitude deconvolution from the RSO sub-pixel position, and then estimate the RSO parallax and RSO orbital displacement to obtain a body frame RSO vector estimate.

Since the star tracker is a sequential attitude estimation instrument, attitude deconvolution is performed sequentially at each image frame. The attitude deconvolution process applies an attitude determination method on the current image star measurements and previous (reference) image star measurements within an image sequence. The reference image contains the desired camera boresight into which other images will be deconvoluted. All the star and RSO measurements in subsequent images will be rotated into this chosen image reference frame. This achieves a scenario in which the camera boresight is artificially stationary in an inertial frame, such that the stars remain fixed and the attitude deconvoluted motion of RSOs is present in the image.

After attitude deconvolution, RSO angular displacement is an orthographic projection of its sidereal motion. Sidereal motion is the motion of an object relative to the stars, which are considered fixed due to the large distances from the objects to the stars. Earth's rotation of 23 h, 56 min, and 4.09 s is a sidereal day, compared to the 24-hour synodic day relative to the Sun. At this step, we attempt to estimate the distance from the host satellite to the RSO using parallax. Parallax is the relative displacement of foreground objects from two different points of observation relative to the background. Knowing the host satellite's displacement between two image frames allows us to estimate the distance to the RSO by observing its pixel position displacement [13].

Previous works on angular velocity estimation [20][21] and a vision-based navigation system [20][22] demonstrate that the body frame RSO vector can be estimated using a star tracker–like sensor. In our approach, we divide Fig. 1(b) by concentric circles referenced to the star tracker boresight as shown in Fig. 5. Highlighted in red is the inertial RSO position displacement projected onto the image plane, in green the inertial host satellite position displacement projected onto the image plane as a unit vector, and in blue the combination of the previous two vectors to result in the actual RSO position displacement as we observe from the attitude deconvoluted images. The unit vector projection of the host satellite position displacement represents the direction along which the parallax effect takes place. The magnitude of the parallax displacement is dependent on the distance to the RSO, whereas the direction in which this magnitude is applied stays consistent for all RSOs in an image sequence. This is because the direction of the parallax effect is inversely correlated to the host satellite's inertial displacement. We describe our algorithm for parallax estimation and deconvolution in section 3.

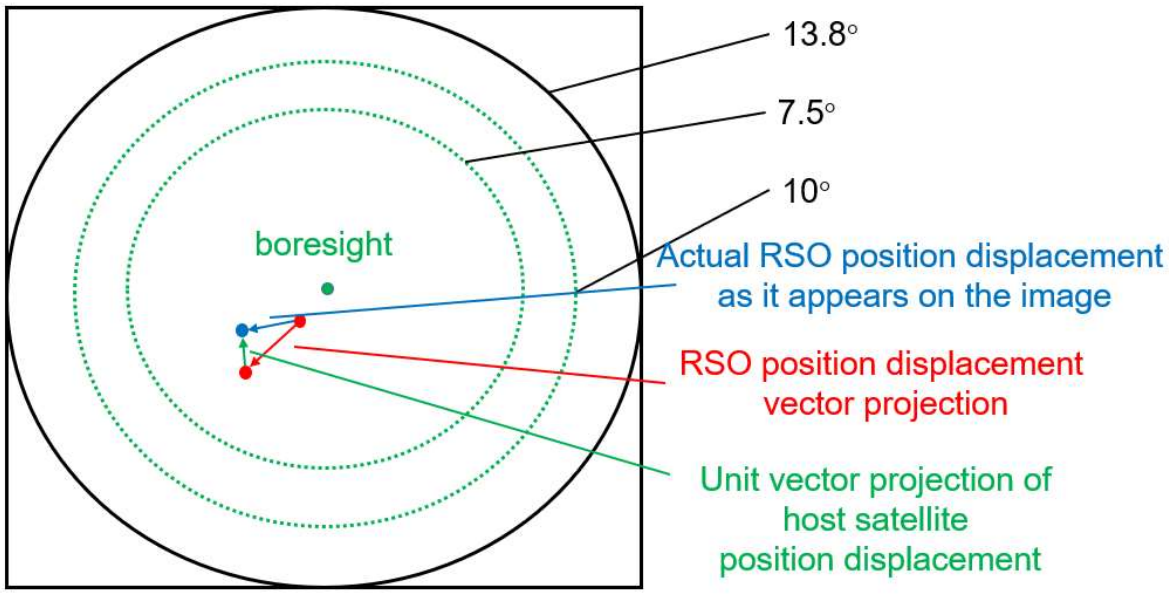

Fig. 5 The effect of parallax on the RSO position displacement projected on the image plane

In section 1 of this paper, we described how we implement our methodology. Section 2 describes how our R-CNN algorithm works and the accuracy it achieves. Section 3 describes how we estimate attitude and attitude deconvolution and estimate the parallax and position state vectors of RSOs. In Section 4, we discuss the results from our implementation, and in Section 5 we highlight our conclusions and consider relevant future work.

2. MACHINE LEARNING ALGORITHM FOR IMAGE SEQUENCE CHARACTERIZATION

In order to detect RSOs in the star field images, a novel R-CNN algorithm was developed using synthetic and simulated images. The algorithm design is divided into two parts: individual image characterization as a CNN and characterized image sequencing using recurrent neural networks (RNN).

Individual image characterization begins with object detection, which is dependent on various parameters that affect the signal-to-noise ratio or the brightness magnitude of the object. The minimum visual magnitude of a detectable RSO using the SBOIS, as discussed in [5], is 7.5 for 10 m–sized RSOs and 6 for 10 cm–sized RSOs. Visual magnitude of a star is a way of rating a star's brightness as seen from Earth. It is logarithmic, with the dimmest stars we can see rated as magnitude 6 and easily visible stars as magnitude 1. The lower the number, the brighter the object, with the Sun rated as –26. The variance in the detection of RSOs by visual magnitude is due to effects of angular velocity, object albedo, host satellite spin rate, background or instrument noise sources, and distance to RSO. In low-resolution images (256 × 256 pixels) RSOs are bounded within 3 × 3 macro images.

A CNN-based binary classifier, shown in Fig. 6, was designed to perform image segmentation to classify each macro-image for whether it contained an object. The macro is used to perform a set of convolution operations across multiple parallel channels, with each channel being a filter designed to identify a feature of the macro space. The feature representation indicators (for RSOs and stars) are used as inputs to train a fully connected neural network layer. After training over 7000 labeled images generated by the SBOIS, the binary classifier was used to make predictions on whether previously unseen macros contain objects. The binary classifier achieved an average accuracy of 96% in detecting stars and RSOs with visual magnitude of 6 or less. Once objects were detected, the next step was estimating the sub-pixel position of the center of that object within the macro-image.

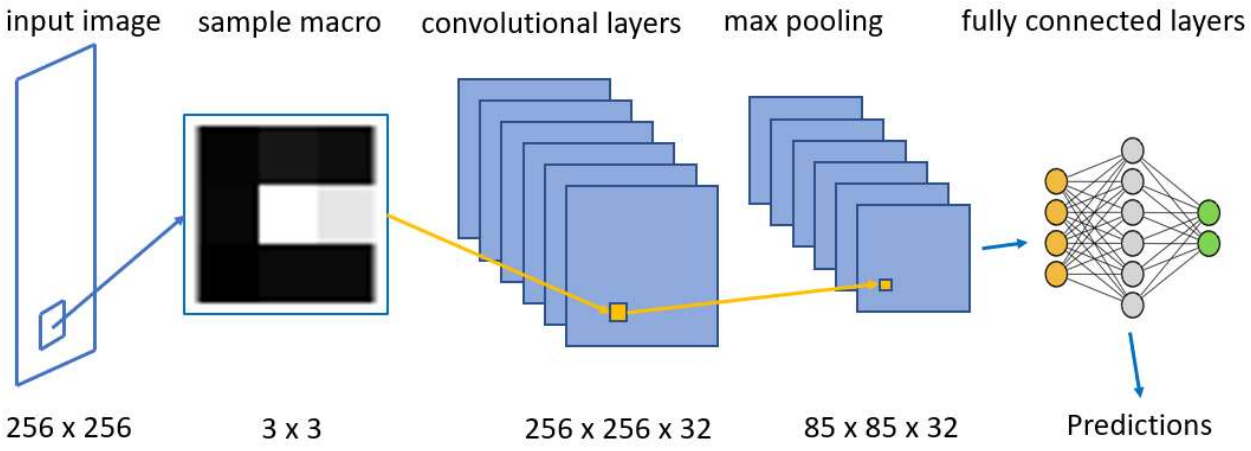

Fig. 6 Layers of a CNN binary classifier used during training

As mentioned previously, the point spread function of the optical sensor causes an RSO with an angular size of 20 arcseconds to occupy up to 20 arcminutes of the field of view. In addition, the low-resolution and high field-of-view properties of the star tracker mean that each pixel accounts for 6.6 arcminutes, further limiting the accuracy of the sub-pixel position estimation. As a workaround for this, star trackers implement centroiding algorithms, described in [23][24], to improve the sub-pixel estimation of a star. The centroiding algorithms work best for stars, since their position displacement is entirely representative of host satellite attitude change. RSOs, however, can have a displacement of up to 0.7 km within the 0.1 s exposure time of the star tracker, potentially adding error to previously

mentioned centroiding algorithms. Our approach is to extend the CNN classifier framework, used to detect objects, by including a regression component. Regression, in the scope of machine learning, is the output of a neural network model, which is like a classifier, but instead of discreet classification labels the fully connected layers output a continuous value as a prediction.

In our context, the continuous output values are the *x* and *y* sub-pixel position of the RSO, and star represented by the blue dot in Fig. 7. In order to train the network for regression, the amount of training data available from the simulator, despite many thousands of object detections, is inadequate. Therefore, a synthetic macro generator was designed to produce training data for regression applying the Monte Carlo simulation method. There is a host of factors that affect how the object appears on an image, such as object albedo, relative velocity, background noise, distance to object, size of object, exposure time, and the point spread function of the optical instrument. In addition, because of the 0.1 s exposure time, RSOs can have a large relative orthogonal angular displacement, whereas stars tend to have very little (on the order of 10^{-5} pixels). Object position center, streak vector (angular displacement during exposure time), macro size, object albedo factor, background noise, and point spread convolution function are the chosen variable parameters of the synthetic generator.

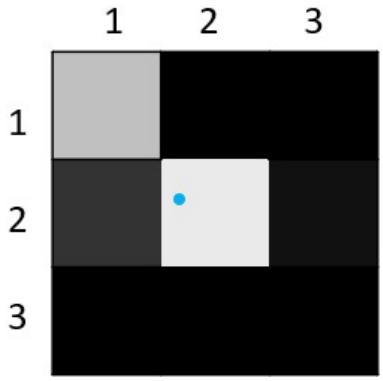

Fig. 7 An example of our CNN-based regression to estimate the sub-pixel position of a detected object

The synthetic generator performs combinations over a specified range of input parameters to generate over 18 million macros, with respective sub-pixel labels for training. Post training, we re-evaluate our network's predictions on synthetic and simulated images, results of which are shown in Table 1. With the accuracy of our sub-pixel prediction known, the angle θ described in Fig. 2 is now well understood.

Table 1 Sub-pixel estimation accuracy of CNN regression training

Object label	Synthetic image root mean squared error	Simulated image root mean squared error
Star	5×10^{-4} pixels or 1.8×10^{-1} seconds of arc	4×10^{-2}pixels or 16 seconds of arc
RSO	2×10^{-3} pixels or 8×10^{-1} seconds of arc	6×10^{-2} pixels or 24 seconds of arc

The final component of the machine learning algorithm is an RNN, the temporal component of the spatiotemporal vector. RNNs use internal state or memory to make predictions on a set of sequential data. By characterizing the position displacement of an object over an image, the R-CNN predicts where an object shows up in the next frame, making it easier to classify between multiple objects with crossing paths. Specifically, our R-CNN implements the long short-term memory units to distinguish between RSO tracks using image co-segmentation techniques. With the conversion from image sequence to spatiotemporal representation handled by the machine learning algorithm, we can now try to estimate the RSO position.

3. STATE VECTORS FROM IMAGE SPACE

In order to use an attitude estimation algorithm, a projection method must be defined for the conversions between 2D image coordinates and 3D unit vectors. In this paper, an orthographic projection was used for both vector-to-pixel and pixel-to-vector conversions, shown below. An orthographic projection uses projection lines that are orthogonal to the projection plane.

$$x=\cos(\phi)\sin(\lambda-\lambda_0) \tag{1}$$

$$y=\cos(\phi_0)\sin(\phi)-\sin(\phi_0)\cos(\phi)\cos(\lambda-\lambda_0) \tag{2}$$

where $\phi \equiv$ latitude, $\lambda \equiv$ longitude, $\phi_0 \equiv$ boresight latitude, $\lambda_0 \equiv$ boresight longitude

$$\phi=\sin^{-1}\left(\cos(c)\sin(\phi_0)+\frac{y\sin(c)\cos(\phi_0)}{\rho}\right) \tag{3}$$

$$\lambda=\lambda_0+\operatorname{atan2}\left(x\sin(c),\ \rho\cos(\phi_0)\cos(c)-y\sin(\phi_0)\sin(c)\right) \tag{4}$$

$$\rho=\sqrt{x^2+y^2} \text{ and } c=\sin^{-1}(\rho) \tag{5}$$

Attitude determination algorithms, QUEST included, begin with Wahba's problem [25]. Wahba's problem finds the rotation between two frames, body and inertial, given two sets of vectors within these frames. The solution seeks to minimize the least squares residual of the following cost function:

$$J(A)=\frac{1}{2}\sum_{i=1}^{N} a_i\ |b_i-Ar_i|^2 \tag{6}$$

where N=the total number of vectors, a_i=weights, b_i=body vector,

r_i=inertial vector, A=orthogonal matrix

The choice of weights is often normalized to unity, or the weights are proportional to the inverses of the measurement variances [14]. Once minimized, we can assume *A* is the optimized solution solving the rotation matrix between the body and inertial frames of reference. The implementation of QUEST followed [26][27] from this point on. Reformulate the loss function *J* to the following form:

$$J(A)=\lambda_0-\operatorname{trace}\left(AB^T\right) \tag{7}$$

$$\text{where } \lambda_0=\sum_{i=1}^{N} a_i=1 \text{ , and } B=\sum_{i=1}^{N} a_i b_i r_i^T \tag{8}$$

The loss function can further be modified such that the attitude matrix is parametrized by a unit quaternion:

$$\operatorname{trace}\left(AB^T\right)=q^TKq \tag{9}$$

$$\text{where } K=\begin{bmatrix} S-\sigma I & Z \\ Z^T & \sigma \end{bmatrix},\ \sigma=\operatorname{trace}(B),\ S=B+B^T,\ Z=\begin{bmatrix} B_{23}-B_{32} \\ B_{31}-B_{13} \\ B_{12}-B_{21} \end{bmatrix}$$

Next, the following characteristic equation is solved using the Newton-Raphson method, with unity as a starting value:

$$\lambda^4-(a+b)\lambda^2-c\lambda+(ab+c\sigma-d)=0, \tag{10}$$

$$\text{where } a=\sigma^2-\kappa,\ b=\sigma^2+Z^TZ,\ c=\Delta+Z^TSZ,\ d=Z^TS^2Z,\ \sigma=\frac{1}{2}\operatorname{tr}(S),$$

$$\kappa=\operatorname{trace}\left(\operatorname{adj}(S)\right),\ \Delta=\det(S) \tag{11}$$

Finally, q_{opt} was calculated, representing the optimal quaternion between the body and inertial reference frames:

$$q_{opt}=\frac{1}{\sqrt{\gamma^2+|X|^2}}\begin{Bmatrix}\gamma \\ X\end{Bmatrix} \tag{12}$$

$$\text{where } \gamma=\alpha\left(\lambda+\operatorname{tr}(B)\right)-\det(S),\ X=\left(\alpha I+\beta S+S^2\right)Z,\quad \alpha=\lambda^2-\left(\operatorname{tr}(B)\right)^2+\operatorname{tr}\left(\operatorname{adj}(S)\right),\ \beta=\lambda^2-\operatorname{tr}(B)$$

The root mean squared error was calculated for a 26-image sequence. The average RMSE between 26 images for the spacecraft yaw was 4.95 arcseconds, the pitch was 0.032 arcseconds, and the roll was 4.95 arcseconds, as shown in Fig. 8.

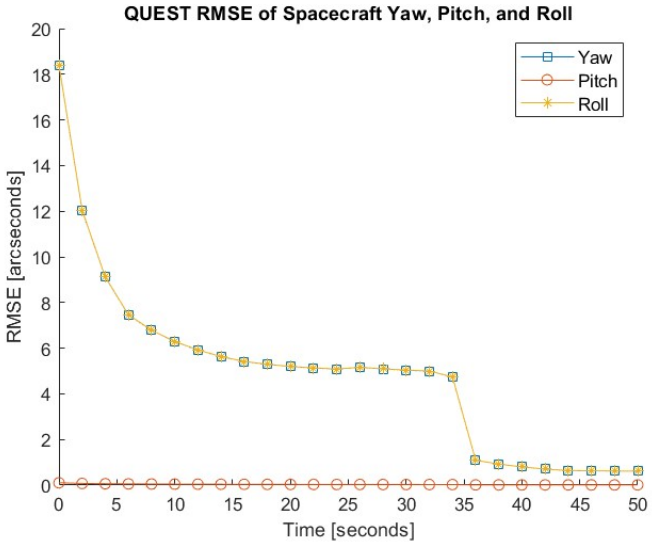

Fig. 8 Attitude determination with QUEST

The attitude deconvolution method first selected the initial image within the sequence as its reference image. It then selected three stars within the current image and verified that all three stars are present within this reference image. Three stars that are within the field of view between the current and reference image is a requirement when using the attitude deconvolution method. Next, an attitude determination method was applied to these three stars within the body frame between both star measurements in the current and reference images. In this paper, we used QUEST for this purpose. The pixel-to-vector conversions used the orthographic projection method. The result of applying QUEST to the star measurements within the same body frame between two images is the attitude change in time between images. The resulting rotation matrix was applied to all star and RSO measurement vectors within the current image. The inverse orthographic projection method was used for the vector-to-pixel conversions. The root-mean-square error was calculated for all 90-star pixel positions in the 26-image sequence and is shown in Fig. 9. After attitude deconvolution of RSOs, we attempt to estimate the parallax.

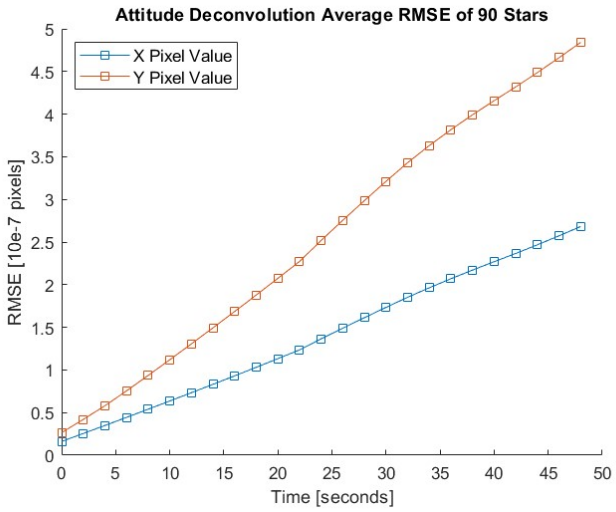

Fig. 9 Attitude deconvolution RMSE for stars

As mentioned, the unit vector of the parallax effect on the RSO is defined by the host satellite's inertial displacement. When this inertial displacement's orthographic projection is laid onto the image plane, it produces a vector like the one shown in green in Fig. 5. We only use the unit vector because magnitude is a function of the distance between the host satellite and the RSO: the closer the RSO, the larger the magnitude.

$$\tan\left(\frac{\theta}{2}\right)=\frac{s}{d} \tag{13}$$

where $\frac{\theta}{2}$=the parallax displacement, s=the host satellite position displacement,

d=the average distance between the RSO and the host satellite

The same relationship exists for estimating the RSO displacement on the image frame due to RSO inertial displacement. Therefore, the unit vector of the parallax is shared among all RSOs. Using the SBOIS auxiliary data on distance to RSO, we estimate the parallax effect magnitude of each RSO, apply it to the unit vector, and compensate for its effects from the RSO sub-pixel positions.

The remaining RSO positions are a representation of attitude deconvoluted and parallax compensated view of an RSO from a stationary observation point in space, the stationary point being the position state vector of the host satellite at the first image frame of a sequence. The deconvolution and compensation results are discussed the section 4.

4. RESULTS

In this section, we follow an 18-image sequence, simulated over 36 s, as we perform attitude deconvolution and parallax compensation for RSO position state vector estimation. The sequence shown in Fig. 10 is a simulation of the FAI imager from February 9, 2014, at 16:13:22 UTC. Red dots represent star sub-pixel positions, and purple dots represent RSOs. As explained earlier, classification between stars and RSOs is relatively easier over image sequences with shorter exposure times.

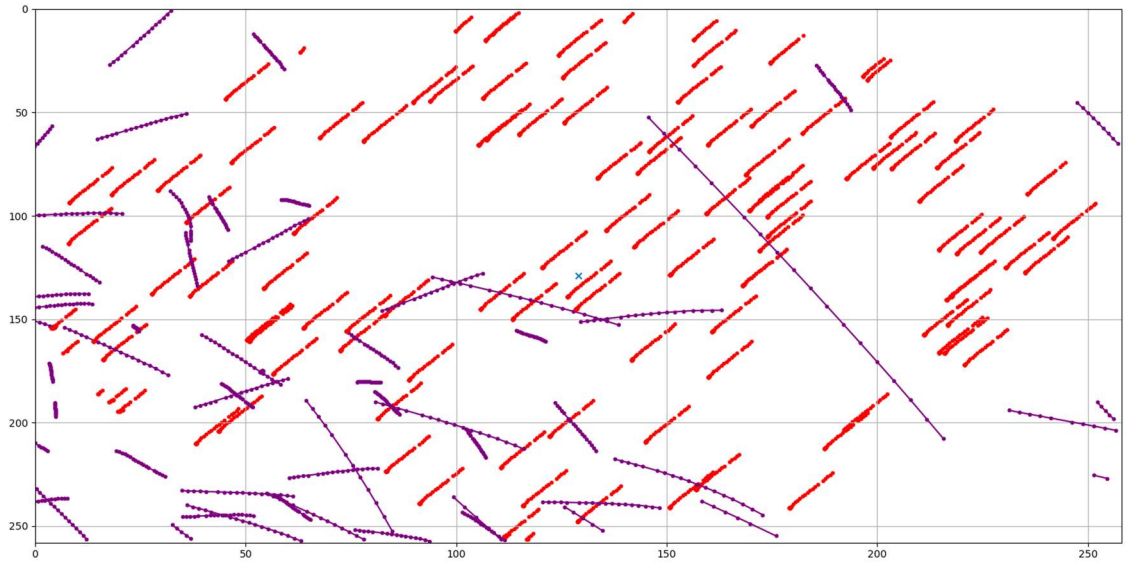

Fig. 10 RSO and star positions over an 18-image sequence; the blue cross is the camera boresight.

After attitude determination is complete, we perform attitude deconvolution on stars. Using International Celestial Reference Frame boresight estimates from attitude determination, the deconvolution brings the stars back to their initial position in the first frame, as seen in Fig. 11. Red represents star positions in the original image sequence, green represents attitude deconvoluted star positions, and in blue we show the boresight cross track motion.

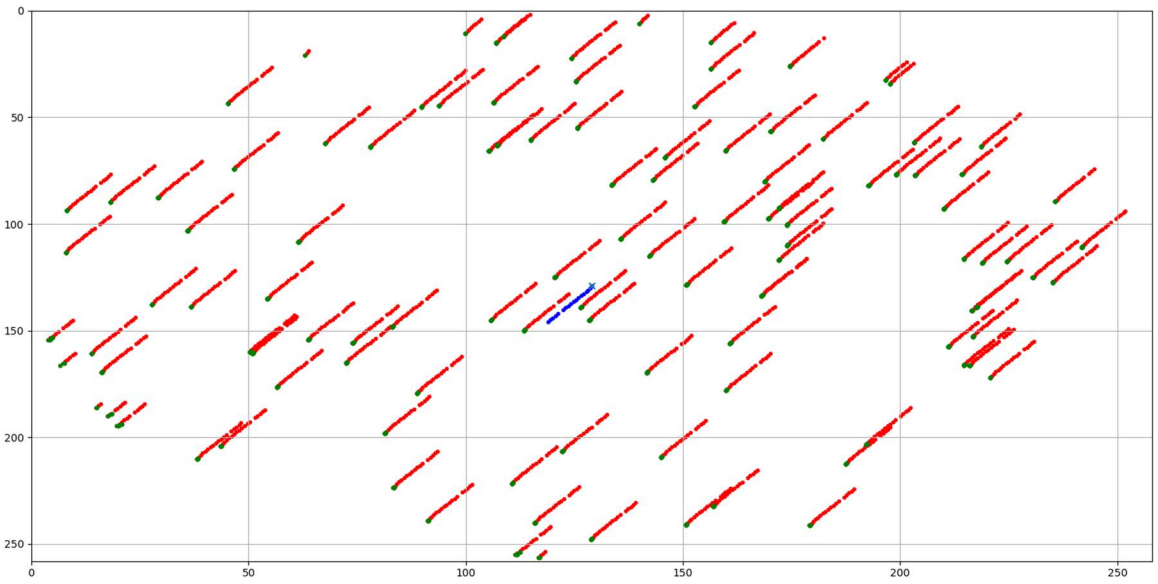

Fig. 11 Attitude deconvoluted star positions

In Fig. 12, we perform the same attitude deconvolution on the RSO positions. Purple represents the original positions of the RSOs from the machine learning algorithm, green represents the attitude deconvoluted position and blue is cross track boresight motion.

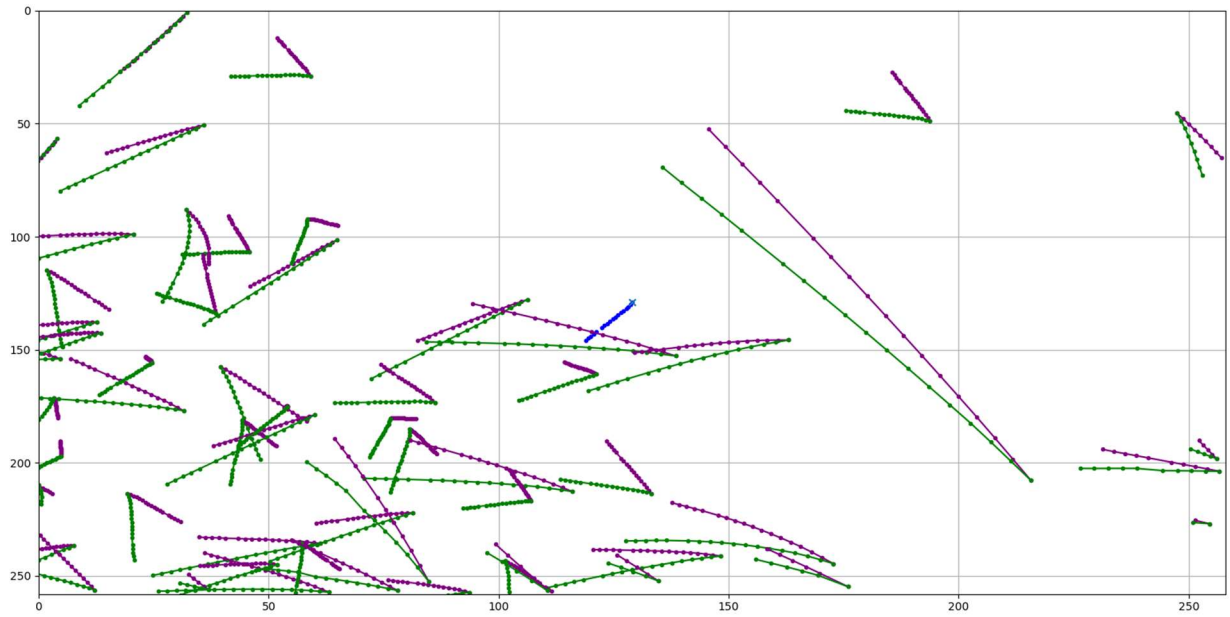

Fig. 12 Attitude deconvoluted RSO positions

In Fig. 13, we combine attitude deconvoluted RSO positions in purple and stars in red, with boresight shift in blue.

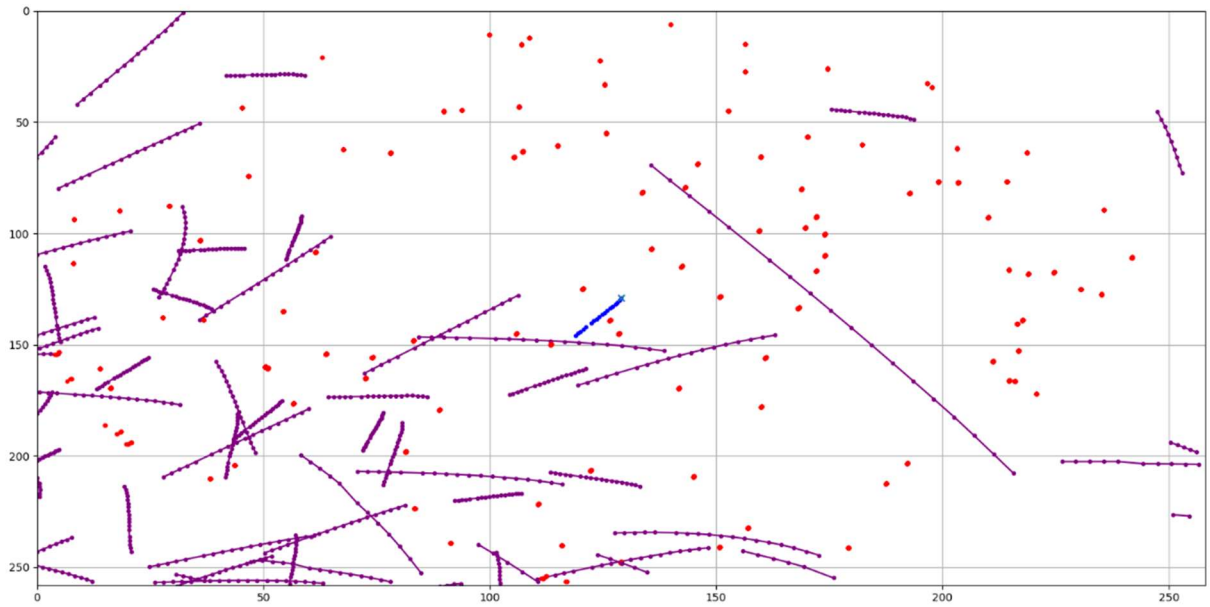

Fig. 13 Attitude deconvoluted RSO and star positions, sidereal motion

In Fig. 14, green represents attitude deconvoluted RSO positions, and blue represents parallax compensated RSO positions (only some tracks are shown for ease of visualization). The red vector originating from boresight represents an orthographic projection of the host satellite's displacement (between two frames) along which the parallax compensation is performed. The vector shown is scaled up by a factor of 10; however, to perform RSO parallax compensation we use the unit vector and determine the magnitude by estimating the distance to the RSO. Fig. 14 illustrates what a host satellite star tracker camera would see if it was stationary with a constant attitude.

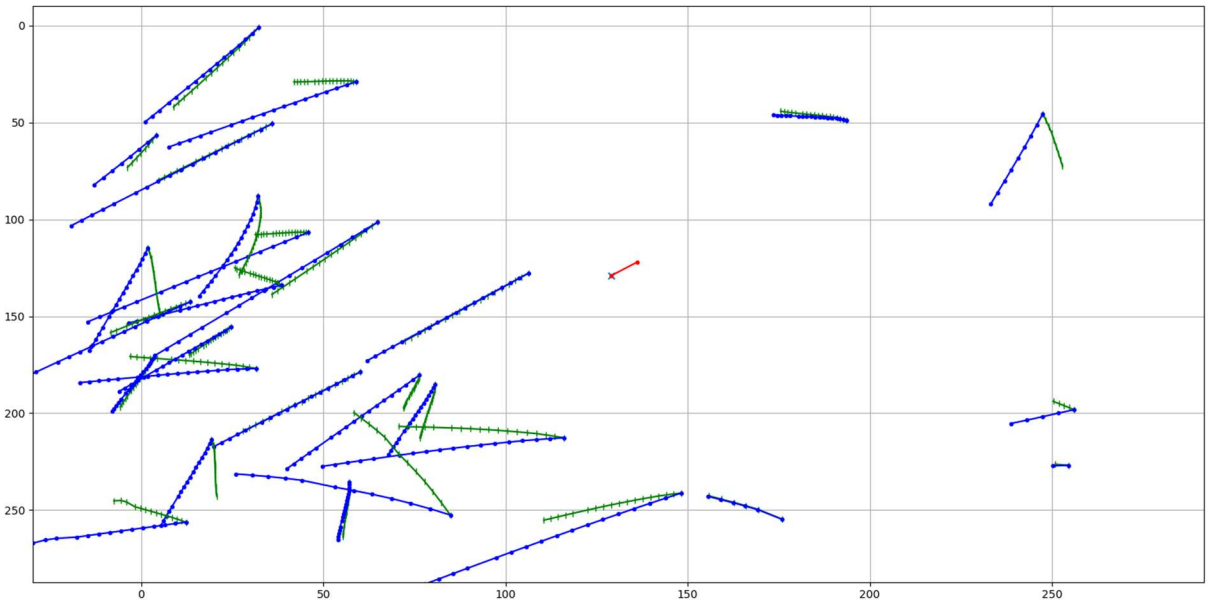

Fig. 14 Parallax-compensated RSO positions

In Fig. 15, the blue curved line represents the tangential relationship between the parallax and the distance to the RSO, whereas the coloured dots represent the distance-to-RSO estimation accuracy after parallax compensation as obtained from the simulated auxiliary data. The RSO cross track displacement along the image frame, or the angular

displacement, is shown in Fig. 15 as a function of the distance to the RSO. The estimation of angle θ referred to in Fig. 2 is described by the *y*-axis in Fig. 15.

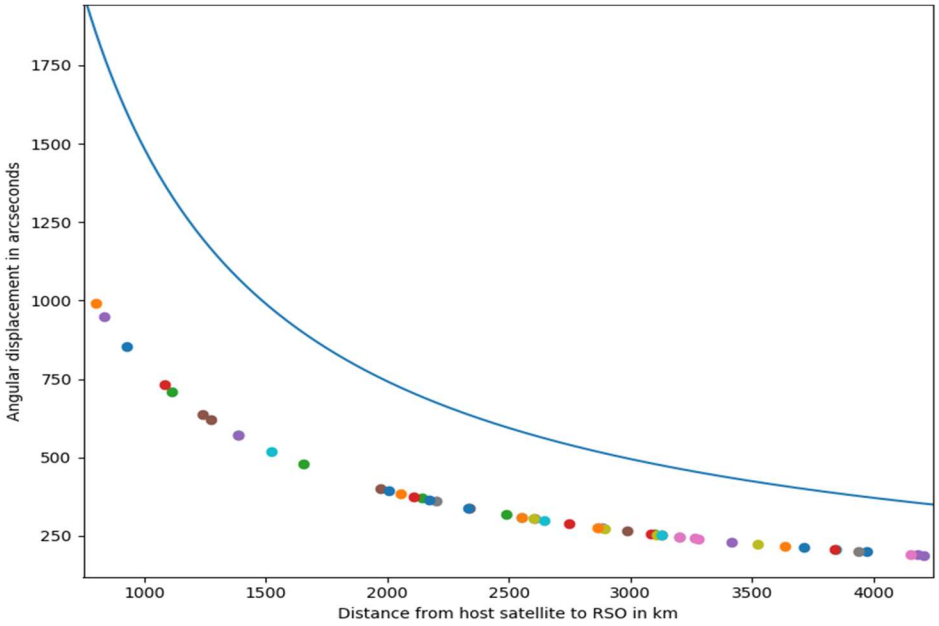

Fig. 15 Cross track RSO position displacement as a function of the distance to RSO

As described in [13], there need to be two separate observations of the same RSO in order to estimate the distance to it. With a frame rate of 0.5 Hz, we know the host satellite is approximately 14.5 km away between two image frames (calculated using simulated orbital data and average orbital velocity in LEO). By using the two image frames as two separate observations of the same RSO, we estimate the distance to the RSO using the parallax compensation method. Using this technique, we estimate the distance to the RSO, or the length of the body frame RSO vector from Fig. 2, to an accuracy of between 255 and 360 km when the RSO is more than 1500 km away facing ram or anti-ram. The error estimation is performed using simulated auxiliary data. When the RSO is less than 1500 km away, the distance estimate is highly inaccurate due to the large parallax displacement. Angular position estimation error, which is also a function of the distance between the host satellite and the RSO is approximately 200 seconds of arc in the cross-track direction.

5. CONCLUSIONS AND FUTURE WORK

As an extension to previous work done in [5], in this paper we show that RSO detection, classification, and tracking can be performed using low-resolution star tracker imagery as described in Section 2. This research signifies the relevance of geographically distributed low-resolution space-based imagery as a potential contributor to SSA. Described in Section 3 is our approach to RSO position estimation using a single low-resolution star tracker. In conclusion, the research performed establishes that tracking RSOs and estimating their positions are achievable using low-resolution space-based imagery. We used a custom SBOIS [6] to generate images, we designed a novel machine learning architecture to process these images, and we used attitude deconvolution and parallax compensation techniques to estimate an RSO's position relative to the host satellite. Using the parallax compensation method, we determined the host satellite's orientations, as in [6], where RSO position estimation is done most accurately. When facing ram or anti-ram, the average accuracy of our estimate of the distance between the RSO and the host satellite is 300 km when the distance is larger than 1500 km. In the cross-track direction, our position estimation error is 200 seconds of arc. The algorithm developed does not require the star tracker to be a dedicated or active SSA sensor, thereby applicable to most satellites. Since it is standard for most satellites to have a star tracker camera, vast amounts of low-resolution space-based images can be sourced for the further development of this algorithm.

As part of our future work, we identify several different areas of research that can improve our results and the accuracy of RSO orbital estimation. Single-point observation or monocular vision of RSOs is the biggest factor of error in position estimation. Combining multi-point observations of RSOs can drastically reduce distance estimation error. Multiple space sensors or space and ground sensor integration is part of our future objective. We also identify several areas of research, in the scope of machine learning, which perform depth estimation using monocular vision [28]. In addition, simulated generative adversarial networks (SimGANs) can be used for image data generation, training, and testing efficiency from variably sourced images in order to further leverage the capabilities of the SBOIS. For additional algorithm development using real images, images from two different sources will be collected and processed to demonstrate the position estimation accuracy.

6. REFERENCES

[1] April, J. (2014). Nanosat employment: a theoretical CONOPS for space object identification NAVAL POSTGRADUATE.

[2] Liebe, C. C. (1995). Star trackers for attitude determination. IEEE Aerospace and Electronic Systems Magazine, 10(6), 10-16.

[3] John D. Vedder, Star Trackers, Star Catalogs, and Attitude Determination: JOURNAL OF GUIDANCE, CONTROL, AND DYNAMICS Vol. 16, No. 3, May-June 1993

[4] Jinchun Wang and Joohwan Chun-, "Attitude Determination Using a Single-Star Sensor and a Star-Density Table JOURNAL OF GUIDANCE, CONTROL, AND DYNAMICS Vol. 29, No. 6, November–December 2006

[5] Clemens, S., Lee, R., & Harrison, P. (2018). Feasibility of Using Commercial Star Trackers for On-Orbit Resident Space Object Detection Warren Soh.

[6] R. Clark and R. Lee, "Parallel Processing for Orbital Maneuver Detection.," Advances in Space Research , 2020.

[7] B. Jia, K. D. Pham, E. Blasch, Z. Wang, D. Shen and G. Chen, "Space object classification using deep neural networks," 2018 IEEE Aerospace Conference, Big Sky, MT, 2018, pp. 1-8.

[8] R. Linares and R. Furfaro, "Space Object classification using deep Convolutional Neural Networks," 2016 19th International Conference on Information Fusion (FUSION), Heidelberg, 2016, pp. 1140-1146.

[9] Leon Muratov, Timothy Perkins, Marsha Fox, Xuemin Jin, Paul LeVan, "Use of AI for Satellite Model Determination from Low Resolution 2D Images," Proceedings of the Advanced Maui Optical and Space Surveillance Technologies Conference, Wailea, Maui, Hawaii, September 17-20, 2019.

[10] Zimmer, P., McGraw, J. T., & Ackermann, M. R. (2018). Real-time optical space situational awareness of low-Earth orbit with small telescopes. *AMOS Conference*.

[11] Cruces, L. (2019). Streak detection in wide field of view images using Convolutional Neural Networks (CNNs) Luis Varela and Laura E . Boucheron Klipsch School of Electrical Engineering New Mexico State University Nick Malone and Nicholas Spurlock Tau Technologies Albuquer.

[12] Scott, R., & Thorsteinson, S. (2018). Key Findings from the NEOSSat Space-Based SSA Microsatellite Mission. *Advanced Maui Optical and Space Surveillance Technologies Conference*. Retrieved from www.amostech.com

[13] Tompkins, J., Cain, S., & Becker, D. (2019). Near earth space object detection using parallax as multi-hypothesis test criterion. *Optics Express*, *27*(4), 5403. https://doi.org/10.1364/oe.27.005403

[14] F. Landis Markley. Daniele Mortari. "HOW TO ESTIMATE ATTITUDE FROM VECTOR OBSERVATIONS"

[15] F. Landis Markley. John L. Crassidis. "Fundamentals of Spacecraft Attitude Determination and Control." 2014.

[16] Jack A. Tappe. “DEVELOPMENT OF STAR TRACKER SYSTEM FOR ACCURATE ESTIMATION OF SPACECRAFT ATTITUDE”. 2009.

[17] Serkan Dikmen. “Development of Star Tracker Attitude and Position Determination System for Spacecraft Maneuvering and Docking Facility”. 2016.

[18] Mcquaid, I. W. (n.d.). AUTONOMOUS ASSOCIATION OF GEO RSO OBSERVATIONS USING DEEP.

[19] Dikmen, S. (2016). Development of Star Tracker Attitude and Position Determination System for Spacecraft Maneuvering and Docking Facility.

[20] İpek, M. (2017). Satellite Orbit Estimation Using Kalman Filters, (February), 134. https://doi.org/10.13140/RG.2.2.26276.53122

[21] Liu, H. B., Yang, J. C., Yi, W. J., Wang, J. Q., Yang, J. K., Li, X. J., & Tan, J. C. (2012). Angular velocity estimation from measurement vectors of star tracker. *Applied Optics*, *51*(16), 3590–3598. https://doi.org/10.1364/AO.51.003590

[22] Woffinden, D. C., & Geller, D. K. (2009). Observability criteria for angles-only navigation. *IEEE Transactions on Aerospace and Electronic Systems*, *45*(3), 1194–1208. https://doi.org/10.1109/TAES.2009.5259193

[20] Zhang, L., Yang, H., Lu, H., Zhang, S., Cai, H., & Qian, S. (2014). Cubature Kalman filtering for relative spacecraft attitude and position estimation. *Acta Astronautica*, *105*(1), 254–264. https://doi.org/10.1016/j.actaastro.2014.09.007

[23] Wei, X., Xu, J., Li, J., Yan, J., & Zhang, G. (2014). S-curve centroiding error correction for star sensor. *Acta Astronautica*, *99*(1), 231–241. https://doi.org/10.1016/j.actaastro.2014.03.002

[24] Wan, X., Wang, G., Wei, X., Li, J., & Zhang, G. (2018). Star centroiding based on fast gaussian fitting for star sensors. *Sensors (Switzerland)*, *18*(9). https://doi.org/10.3390/s18092836

[25] Markley, Landis. (1999). 30 Years of Wahba's Problem.

[26] F. Landis Markley. John L. Crassidis. “Fundamentals of Spacecraft Attitude Determination and Control”. 2014.

[27] Yang Cheng. Malcolm D. Shuster. “An Improvement to the implementation of the QUEST algorithm.” 2014.

[28] Zhao, C. Q., Sun, Q. Y., Zhang, C. Z., Tang, Y., & Qian, F. (2020). Monocular depth estimation based on deep learning: An overview. Science China Technological Sciences. https://doi.org/10.1007/s11431-020-1582-8